RESEARCH ARTICLE | FEBRUARY 15 2002

Ab initio adiabatic and diabatic energies and dipole moments of the KH molecule

Neji Khelifi; Brahim Oujia; Florent Xavier Gadea

J. Chem. Phys. 116, 2879–2887 (2002)
https://doi.org/10.1063/1.1436467

Ab initio adiabatic and diabatic energies and dipole moments of the KH molecule

Neji Khelifi and Brahim Oujia
Laboratoire de Physique Quantique, Université du Centre, Faculté des Sciences de Monastir, route de Kairouan 5019, Monastir, Tunisie

Florent Xavier Gadea[a)]
Laboratoire de Physique Quantique, UMR5626 du CNRS, Université Paul Sabatier, 118 route de Narbonne, 31062 Toulouse Cedex 4, France

(Received 10 May 2001; accepted 28 November 2001)

An *ab initio* adiabatic and diabatic study of the KH molecule is performed for all states below the ionic limit [i.e., K ($4s$, $4p$, $5s$, $3d$, $5p$, $4d$, $6s$, and $4f$)+H($1s$)] in $^1\Sigma^+$ and $^3\Sigma^+$ symmetries. Adiabatic results are also reported for $^1\Pi$, $^3\Pi$, $^1\Delta$, and $^3\Delta$ symmetries. The *ab initio* calculations rely on pseudopotential, operatorial core valence correlation, and full valence CI approaches, combined to an efficient diabatization procedure. For the low-lying states, our vibrational level spacings and spectroscopic constants are in very good agreement with the available experimental data. Diabatic potentials and dipoles moments are analyzed, revealing the strong imprint of the ionic state in the $^1\Sigma^+$ adiabatic states while improving the results. The undulations of the diabatic curves and of the triplet–singlet diabatic energy difference which we found positive, as in Hund's rule, are related to the Rydberg functions. As for LiH, the vibrational spacing of the A state is bracketed by our results with and without the improvement taking into account the diabatic representation. Experimental suggestions are also given. © *2002 American Institute of Physics.*
[DOI: 10.1063/1.1436467]

I. INTRODUCTION

Alkali hydrides have been the object of intense theoretical and experimental interest for many years.[1–12] Such molecules are at the intersection of various theoretical and experimental challenges, and now are tractable with high reliability via *ab initio* techniques. Using appropriate methods, it is possible to approach the experimental results with an overall good agreement for the ground and excited states.

Their ground state is known to be of ionic character but dissociates to neutral fragments. A charge-transfer crossing is therefore expected to occur, making this problem attractive for diabatization. The diabatic approach brings physical insight as shown in the previous studies of the LiH molecule,[1,13,14] suggesting further calculations of non Born–Oppenheimer effects such as transitions occurring in collisions,[15–17] the estimation of vibronic effects (vibronic shifts,[12,18–20] nonradiative life time[12,19,20]). In addition, the diabatic picture can be used to improve the accuracy of calculations by overcoming basis set limitations on the electron affinity of H, which is among the main limitations in the *ab initio* approach, particularly for the binding energy of the ground state.[1]

Undulations in the potential of the highly excited states were revealed and analyzed in our previous study of LiH[1] and further confirmed in various recent works.[11,21–24] These undulations were shown to be magnified in the diabatic curves and to be related to intrinsic characteristics of the Rydberg atomic functions. In the present paper we will investigate how these analyses produced for LiH potentials apply to KH.

Although realistic all-electron calculations are now feasible for the KH hydride, we prefer to use the pseudopotential approach for the core and large basis sets of the valence and Rydberg states, which allows accurate descriptions of the highest excited states, allowing also calculations of similar quality for the whole alkali hydride series. The two electrons are then treated at the full configuration-interaction level (here CISD). Core–valence correlation effects are quite important. Here we use the well established operatorial approach proposed by Müller, Flesh, and Meyer.[25]

In this paper we present the first *ab initio* calculations on highly excited states of the potassium hydride molecule, treating nearly all states dissociating below the ionic one (i.e., $4s$, $4p$, $5s$, $3d$, $5p$, $4d$, $6s$, and $4f$). The accuracy of the results can be judged by a comparison with the numerous theoretical and experimental data for the two lowest states. In addition to the adiabatic potential curves and dipoles moments, diabatic curves are also derived. A further interest of this work is an improvement of both potential curves and dipole moments related to the H electron affinity correction effects allowed by the use of an efficient diabatization method.

Therefore a rather complete set of data is presented about the KH molecule from ground to highly excited states including adiabatic potential energy in $^1\Sigma^+$, $^3\Sigma^+$, $^1\Pi$, $^3\Pi$, $^1\Delta$, $^3\Delta$ and permanent dipole and transition dipole moments, as well as potential electronic couplings, for the corresponding diabatic states. This set of data will be further used to

a)Electronic mail: gadea@irsamc.ups-tlse.fr

TABLE I. Calculated transition energies and ionization potential (IP) of the K atom (cm^{-1}).

State	This work	Experiment[a]
$4s$	0	0
$^2P(4p)$	13023.6	13030.1
$^2S(5s)$	21014.1	21026.8
$^2D(3d)$	21535.3	21535.3
$^2P(5p)$	24717.5	24716.0
$^2D(4d)$	27401.9	27397.4
$^2S(6s)$	27446.2	27450.7
$^2F(4f)$	28142.2	28127.7
IP	34998.2	35009.8

[a]Reference 28; averaged over m_J values.

perform detailed spectroscopic studies including vibronic effects, radiative and nonradiative life times.

In Sec. II we briefly present the computational method; and give numerical details. Section III is devoted to the presentation and discussion of the diabatic and adiabatic results. In Sec. IV we present the permanent dipole moment for the adiabatic and diabatic representations. Suggestions of spectroscopic interest are proposed in Sec. V. Finally, we summarize our results and conclude in Sec. VI.

II. METHODS

A. Computational details

The potassium is treated as a one-electron system using the nonempirical pseudopotential of Barthelat and Durand,[26] in its semi local form,[4] and as in LiH[1] we used the *ab initio* package developed in Toulouse. For the K atom we used a 8*s*, 5*p*, 5*d*, 2*f* Gaussian basis set appropriate for the K pseudopotential, where diffuse orbital exponents have been optimized to reproduce all the 4*s*, 4*p*, 5*s*, 3*d*, 5*p*, 4*d*, 6*s*, and 4*f* atomic states, while a more restricted basis set has been employed for hydrogen. This 5*s*, 3*p*, 2*d* basis set can be considered as a reasonable compromise, able to describe both neutral and negatively charged (H^-) hydrogen. A larger basis set for H could not be used because of numerical problems during the diabatization process, the main effect of this rather small H basis being an error (405 cm^{-1}) in the H electron affinity, which, however, is corrected due to the diabatic approach used. An extensive range of internuclear distances has been considered, ranging from 2.45 to 1000 bohr, in order to cover all the ionic–neutral crossings in the $^1\Sigma^+$ symmetry.

For the simulation of the interaction between the polarizable K^+ core with the valence electrons and H nucleus a core polarization potential is used, according to the operatorial approach of Müller, Flesh, and Meyer.[25] Following the formulation of Foucrault, Millie, and Daudey[27] cut-off functions with *l*-dependent adjustable parameters are fitted to reproduce not only the first experimental ionization potential but also the lowest excited states of each *l*, namely $^2S(4s)$, $^2P(4p)$, $^2D(3d)$, and $^2F(4f)$ for K. In the present work, the core polarizability of potassium is $\alpha_K^+ = 5.457$ (bohr) (Ref. 27) and the optimized cut-off parameters are $\rho_s = 2.115$, $\rho_p = 2.1125$, $\rho_d = 1.98$ bohrs, and $\rho_f = 2.0$ bohr. The resulting atomic potassium spectrum is reported in Table I; neutral dissociation limits are very accurate for all the 4*s*, 4*p*, 5*s*, 3*d*, 5*p*, 4*d*, 6*s*, and 4*f* states, the largest error being 14.5 cm^{-1} for the 4*f*.

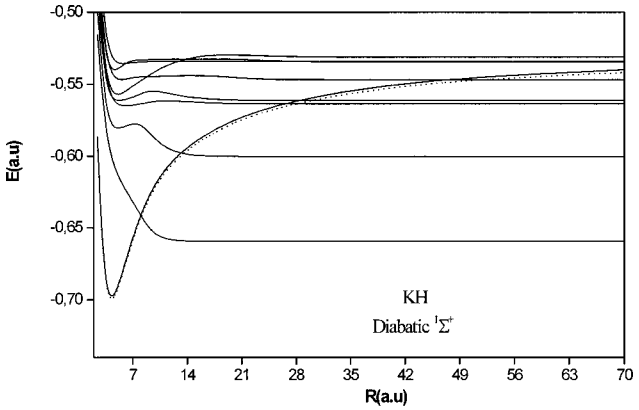

FIG. 1. KH diabatic potential energy curves for the $^1\Sigma^+$ states, method 2; dotted line, the ionic curve corrected for the H electron affinity error.

B. Diabatization

We briefly recall the principal lines of the method used; more details can be found in previous publications.[1,29–31] The strategy is to compute a numerical estimate of the nonadiabatic coupling between the relevant adiabatic states and to cancel it by an appropriate unitary transformation according to the effective Hamiltonian theory.[29,32] The estimate is, however, obtained using the large internuclear intervals used in the molecular calculation instead of infinitesimal ones, and an effective overlap matrix is employed, in order to asymptotically ensure vanishing radial couplings and to get stable results. This nonadiabatic coupling calculation is closely related to an overlap matrix[30,31] between the *R*-dependent adiabatic multiconfigurational states and an R_0 fixed set of reference states. It is shown to be sensitive to the choice of the origin in space, here the K atom. This diabatization method was shown to be among the most effective for molecular *ab initio* calculations.[31]

For the set of reference states, we have explored two possibilities: in the first method the set of reference states are the adiabatic states for a fixed, very large, internuclear distance $R_0 = 1000$ bohr (method 1). In the second method (2) the set of reference states are the diabatic states calculated for the larger neighboring distance. The calculation is performed from the largest distance, where the diabatic states are initialized to the adiabatic ones to the shortest one, similar to an integration scheme. Method 2 was shown to be more effective than 1 in the sense that it leads to smaller residual couplings between the diabatic states.[31] However, method 1 allows for an easy control of the phases since all the effective Hamiltonians for the various distances are computed in the same fixed reference basis set. The two methods are compared in the following section.

III. RESULTS

A. Diabatic results

The results of method 2 are presented in Fig. 1 for the singlet and Fig. 2 for the triplet Σ^+ states. As expected, for

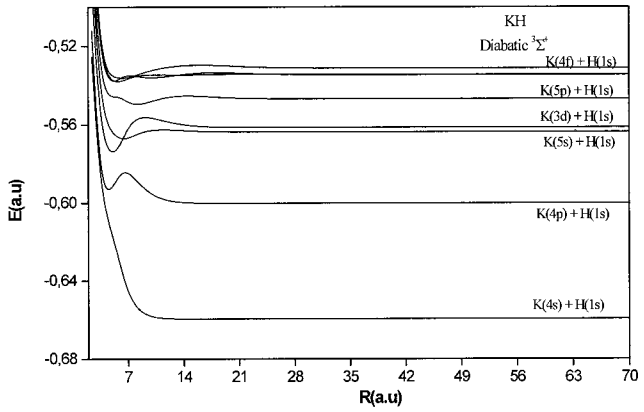

FIG. 2. Kh diabatic potential energy curves for the $^3\Sigma^+$ states, method 2.

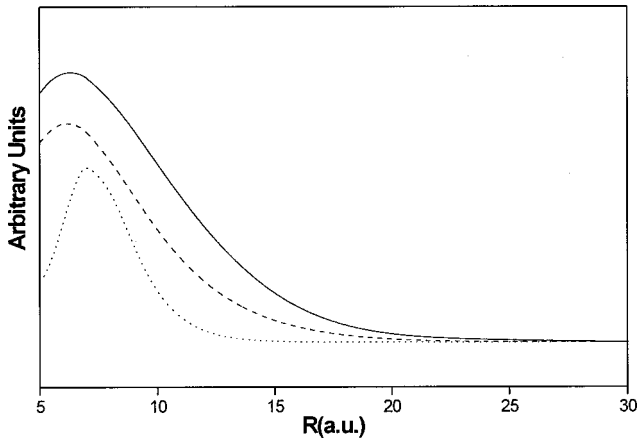

FIG. 3. Triplet–singlet diabatic energy difference (dotted line), coupling integral to the ionic state (dashed line), orbital density $r^2\phi(r)$ (solid line) for the 4*s* state as a function of internuclear distance, method 2.

$^1\Sigma^+$ symmetry, the ionic curve crosses all the neutral ones at different distances, in both methods. The crossing occurs with the 4*s* state around 8 bohr, with the 4*p* around 13 bohr, and with the 5*s* around 26.5 bohr, the others occurring at much larger distances. Inspection of the coupling magnitude corroborates the conclusion (evident from the adiabatic curves) that the crossing become less and less avoided as the ionic curve asymptotically encounters higher-energy Rydberg states at increasing internuclear distances. In Fig. 1 the ionic curve downshifted in energy by the H electron affinity error is also reported as a dotted line while the crossings with the neutral states are pushed to larger distances. The two methods lead to qualitatively similar results, although there are quantitative differences particularly at short distances; we have thus reported here only the results of method 2.

As expected, the ionic curve behaves as $1/R$ at large internuclear distances, with some corrections proportional to $1/R^4$ corresponding to H^- dipolar polarization and also to core–valence interactions. The slope of the neutral curves seems erratic, but their diabatic character which should preserve intrinsic aspects of the Rydberg states, helps the analysis. Similarly to LiH,[1] the energies of the triplet diabatic states are systematically lower than those of the singlet ones, and the lower the energy of the corresponding Rydberg state, the larger the difference. This behavior nicely indicates that the stabilizing interaction with the ionic state has been again removed for all singlet states. It is well known that in the triplet the repulsive electron–electron interactions are minimized, $E_{\text{triplet}}=E_0-K$ (K is the exchange integral, positive for the atoms), with $E_{\text{single}}=E_0+K$, when no coupling with the ionic state is allowed. Thus the diabatic states follow the atomic Hund's rule in both methods.

As in LiH, closer inspection reveals that the location of the maximum of this triplet–singlet energy difference shifts toward large internuclear distances, and the energy difference at the maximum decreases as one goes up in the Rydberg series. This is the behavior expected for the exchange integral (K). As illustrated in Figs. 3 and 4 for the 4*s* and 4*p* states, the triplet–singlet difference, now assigned to an exchange integral, and the neutral–ionic coupling present essentially the same behavior. This coupling (i.e., the hopping integral) is known to be roughly proportional to an overlap integral, as extensively used in an empirical method such as the extended Hückel theory.[33] Here it is the overlap between the doubly occupied ionic 1*s*' orbital of H^- and the Rydberg orbital of potassium ϕ_K^*. Since the 1*s*' orbital is much more localized than the Rydberg one, this overlap $\langle 1s'|\phi_K^*\rangle$ is expected to be closely related to the Rydberg orbital $[r^2\phi(r)]$, except at short internuclear distances where core interactions cause a breakdown of these simple rules. As in LiH, the exchange integral (K) also appears to be closely related to this overlap. The similarity of the three curves (exchange integral, hopping integral, and orbital function), for both methods and the various Rydberg states illustrated in Figs. 3 and 4 reveals clearly the intrinsic characteristics of these potentials and their close relation with the corresponding Rydberg function amplitudes.

In addition, to this exchange integral, which is important mainly for the lowest states, other effects influence these diabatic curves. One is attractive and related to interactions between H and the K^+ core, the other is repulsive and related to the interactions between the Rydberg electron and the H atom. Both triplet and singlet curves are affected by these effects. All curves asymptotically present a repulsive character, which can be quantitatively related to the corresponding Rydberg orbital amplitude. The hydrogen atom interacts re-

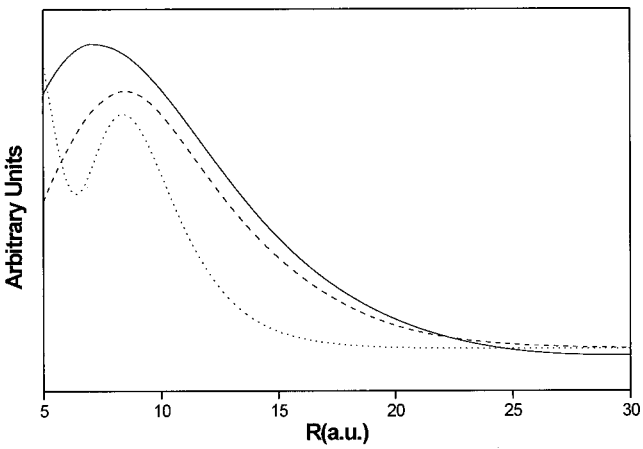

FIG. 4. The same as Fig. 3, but for the 4*p* Rydberg state.

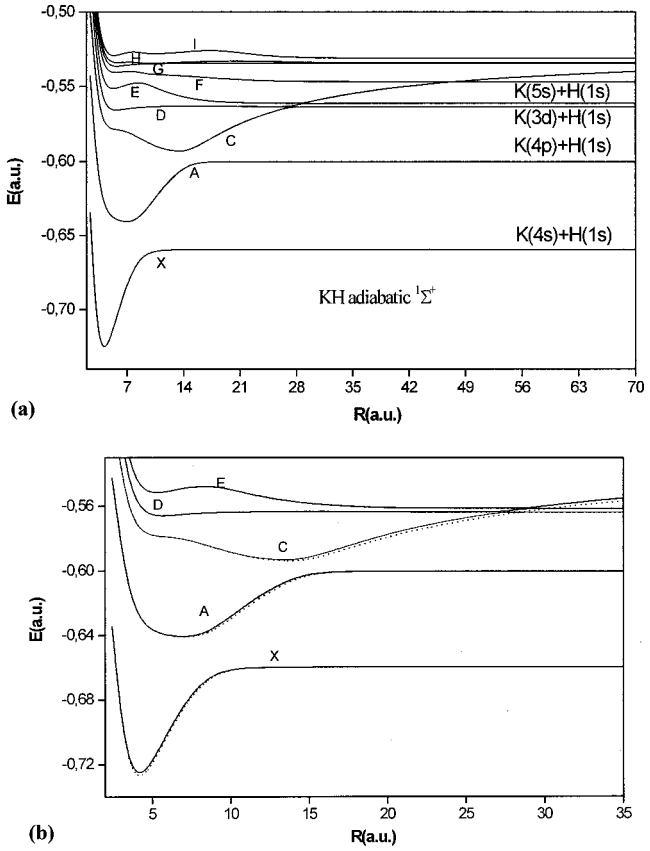

FIG. 5. (a) KH adiabatic potential-energy curves for the $^1\Sigma^+$ states. (b) KH adiabatic potential energy curves for the $X\ ^1\Sigma^+$, $A\ ^1\Sigma^+$, $C\ ^1\Sigma^+$, $D\ ^1\Sigma^+$, and $E\ ^1\Sigma^+$ states with (dotted line) and without (solid line) constant electronic affinity correction of hydrogen.

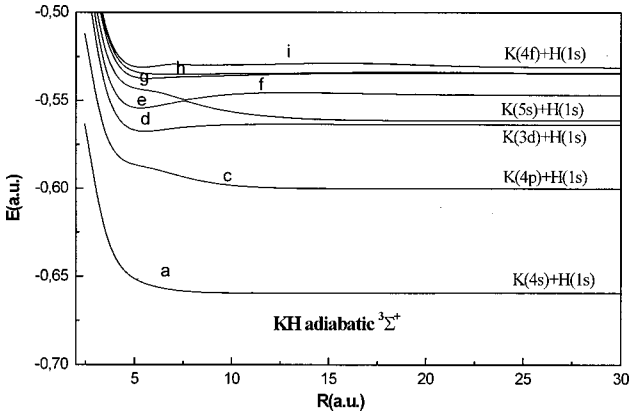

FIG. 6. KH adiabatic potential energy curves for the $^3\Sigma^+$ states.

pulsively with the Rydberg electron with a narrow region of space corresponding to the very localized 1*s* function, and the larger the Rydberg orbital amplitude, the larger this repulsive effect. Accordingly, the quantity $(E_s+E_t)/2$ presents for each Rydberg a maximum at large distances correlated to the maximum of the Rydberg electron density $[r^2\phi(r)]$. As in LiH, both maxima reasonably coincide and clearly shift to large distances following the principal lobe of the Rydberg orbital.

At short distances, as the hydrogen atom penetrates the Rydberg orbital, it is polarized by the field created by the K^+ core and the outer electron. In the Rydberg series, whereas these effects are not clearly apparent for the 4*s* state, since the 4*s* orbital is a valence orbital, both the repulsive and attractive interactions actually take place for the 4*p* state and beyond. For the higher states, the attractive effect dominates at shorter distances and the curves become more and more similar to the KH^+ ones, while the repulsive effect dominates at large distances.

As in LiH[1], the apparently strange behavior of the diabatic states can thus be satisfactorily interpreted by simple arguments, emphasizing again the physical relevance and utility of the diabatization procedure. Furthermore, a quantitative comparison can be made between the diabatic curves and the ones obtained from the Fermi model[34,35] as emphasized recently[36] for LiH and NaH. The comparison between the two diabatization methods shows that there is no essential difference between the two techniques, so we will continue our presentation and discussion based on method 2 only.

B. Adiabatic results and corrections

Figures 5(a), 5(b), and 6 illustrate the adiabatic curves of $^1\Sigma^+$ and $^3\Sigma^+$ symmetries. From the diabatic picture, it is clear that the deep well of the ground state clearly results from the large avoided crossing between the ionic and the 4*s* state. Similarly to LiH, the first excited adiabatic $^1\Sigma^+$ state, usually called the A state, presents a large well formed by the repulsive part of the 4*s* curve at a short internuclear distance, a branch of the ionic curve at an intermediate distance, and the 4*p* asymptote at large distances. In contrast with LiH, the second excited state (C), presents a single minimum, at a large internuclear distance, around the avoided crossing between the repulsive part of the 4*p* state and the ionic one. The third (D) and fourth (E) adiabatic $^1\Sigma^+$ states present double minima, with a well at very large distances and another one at a short distance in the Franck–Condon region of the ground state. Both minima can trap vibrational states.

TABLE II. Bond distances R_e(a.u.) and dissociation energies D_e(cm^{-1}) for the lowest $^1\Sigma^+$ states: (a) uncorrected *ab initio* results; (b) improved results including the correction of H electron affinity.

State		This work (a)	This work (b)	Ref. 11	Ref. 7	Ref. 8	Expt. (Ref. 10)
$X\ ^1\Sigma^+$	R_e	4.19	4.19	4.22	4.28	4.29	4.23
	D_e	14365.0	14750.4	15066.6	13954.1	12905.6	14772.7
$A\ ^1\Sigma^+$	R_e	6.93	7.05	7.01	6.947	7.18	7.11
	D_e	8872.9	8946.3	8811	8711.2	8711.2	8698

TABLE III. Bond distances R_e(a.u.), dissociation energies D_e(cm^{-1}), and transition energy T_e(cm^{-1}) for the higher excited $^1\Sigma^+$ states. Only the improved results (b) are reported.

State	Reference	R_e	D_e	T_e
	(b)	13.63	6584.5	34602.9
$C\ ^1\Sigma^+$	Ref. 11	13.40	6516	
	(b)	5.65	873.5	38393.9
$D\ ^1\Sigma^+$	Ref. 11	5.59	881	
	(b)	5.28	1026.9	41217.0
$E\ ^1\Sigma^+$	Ref. 11	5.24	1012	
	(b)	5.57	1319.9	43475.5
$F\ ^1\Sigma^+$	Ref. 11	5.49	1253	
$G\ ^1\Sigma^+$	(b)	5.67	459.5	44846.7
	Ref. 11	5.60	416	
$H\ ^1\Sigma^+$	(b)	5.83	768.7	45556.5
		9.64	718.5	
	Ref. 11	5.73	546	
		10.30	660	
$I\ ^1\Sigma^+$	(b)	5.37	408.2	46161.4
	Ref. 11	5.41	233	

The crossings of the covalent and ionic states and the magnitude of their interaction completely determine the details of these adiabatic states and the resulting vibrational levels.

In Fig. 5(b), the $^1\Sigma^+$ adiabatic states resulting from the diagonalization of the diabatic effective Hamiltonian using the ionic curve corrected for the H electron affinity error are shown with dotted lines together with the previous adiabatic results. Although only the ionic potential has been modified, almost all adiabatic curves are affected, illustrating again their strong imprint due to the ionic state. Moreover, a difference between the two curves (full line and dotted line) locates a region where the adiabatic state is strongly ionic. The well of the ground state is downshifted in energy while those of the A and higher states are enlarged. These results which use an improved ionic potential will be hereafter referred to as improved results.

It is interesting to examine how the improvement taking into account the diabatic representation modifies the spectroscopic constants of the $^1\Sigma^+$ states reported in Tables II and III. The binding energy of the ground state (Table II) is considerably improved due to the correction of the ionic curve, indicating that the hydrogen electron affinity is an important parameter in the quality of *ab initio* calculations for the alkali hydrides. For the A state (Table III) this correction improves the equilibrium distance which is underestimated in the uncorrected *ab initio* calculation. For higher excited states, no experimental data exist, thus in Table III our results are compared only with the most recent *ab initio* calculation.[11] The two sets of results are consistent, our equilibrium distances being generally shorter and our binding energies somewhat larger.

As can be seen in Table II, our improved results for the binding energy and the equilibrium distance are in good agreement with the experimental data, being better than the previous results and comparable to the most recent one.[11] Compared to the experimental results, our equilibrium distances are shorter, as is also the case in the calculation of Lee *et al.*;[11] both *ab initio* approaches use pseudopotentials and operatorial core valence correlation estimates, while some repulsive effects are clearly underestimated here as in Ref. 11. Solving numerically the vibrational Schrödinger equation, with the improved (uncorrected *ab initio*) adiabatic potentials, we get 26 (25) vibrational levels for the ground state, 37 (36) for the A state, and 58 (55) for the C state.

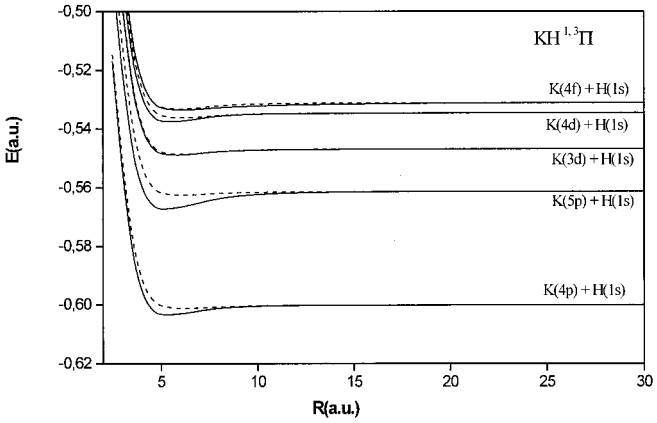

FIG. 7. KH adiabatic potential-energy curves for the $^1\Pi$ (solid line) and $^3\Pi$ (dashed line) states.

The improvement also has an important effect on the vibrational spacing, particularly for the A state, as in LiH.[1] As can be seen in Fig. 7, this correction has no significant effect on the vibrational progression of the ground state since the whole potential curve (mainly ionic) has been slightly downshifted, except for the highest levels, close to the avoided crossing and where the improved results agree better with the experimental spacings. However, for the $A\ ^1\Sigma^+$ state only the long-range ionic branch is changed, and the well is enlarged, producing a lowering of all vibrational level spacings by several cm^{-1}. Without any correction, almost all our vibrational level spacings ($G_{v+1}-G_v$) were larger than the experimental ones, indicating that the ionic branch was not attractive enough. With the correction, the vibrational level spacings are now almost all slightly lower than the experimental ones, indicating that the ionic curve becomes somewhat too attractive and the correction somewhat too large. As shown in Fig. 8, the experimental results for the

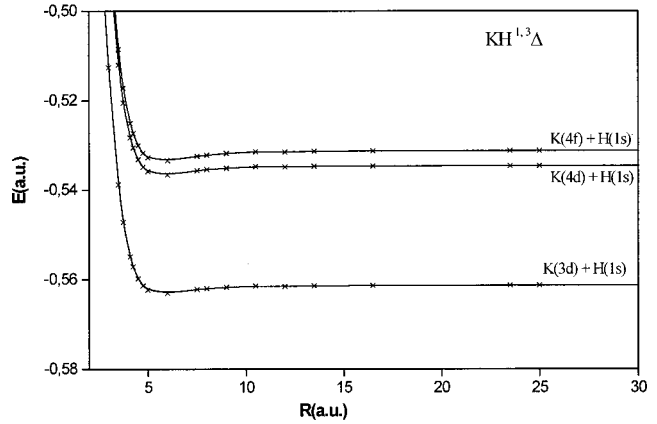

FIG. 8. KH adiabatic potential-energy curves for the $^1\Delta$ (solid line) and $^3\Delta$ (crosses) states.

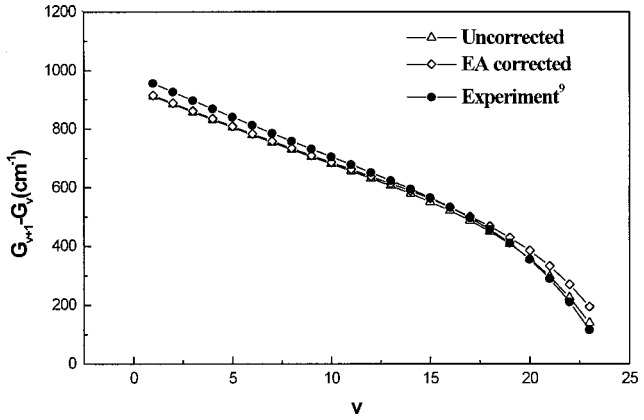

FIG. 9. Vibrational level spacings of the $X\ ^1\Sigma^+$ state of the KH molecule.

$A\ ^1\Sigma^+$ state are bracketed by our results with and without the constant correction, showing that the H electron affinity provides the dominant residual error.

The triplet states (Fig. 6) present smoother and essentially repulsive behavior, as they are not perturbed by the ionic state. The curve dissociating in 3*d* is strongly repulsive even at large distances and leads to an avoided crossing with the curve dissociating in 5*p*. This avoided crossing produces the well in the *e* and *f* states.

Figures 9 and 10 illustrate the singlet and triplet adiabatic Π and Δ states. Since these symmetries involve orbitals perpendicular to the axis of the molecule, which overlap only loosely, the adiabatic curves are rather flat. The singlet and triplet adiabatic Δ curves are almost degenerate. The spectroscopic constants (R_e, D_e, and T_e) of the bound states are given in Table IV. For the B state (the lowest $^1\Pi$) we get 7 vibrational levels with spacing 215.3, 184.2, 121.6, 67.1, 21.4, and 5.6 cm^{-1}.

IV. PERMANENT AND TRANSITION DIPOLE MOMENTS IN ADIABATIC AND DIABATIC REPRESENTATIONS IN Σ SYMMETRY

A. Permanent dipole moments

The permanent dipoles are illustrated in Figs. 11 ($^1\Sigma^+$) and Fig. 12 ($^3\Sigma^+$) for the adiabatic states and in Fig. 13 ($^1\Sigma^+$ method 2) for the diabatic states. We considered a large range of internuclear distances because we expected interesting features to arise from a global picture involving the highly excited states which become ionic at large internuclear distances.

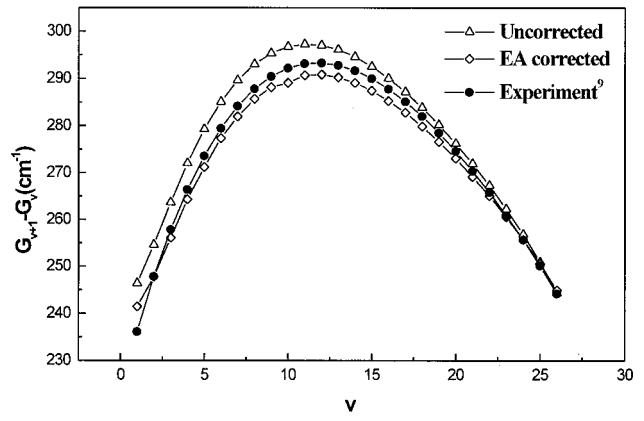

FIG. 10. Vibrational level spacing of the $A\ ^1\Sigma^+$ state of the KH molecule.

TABLE IV. Bond distances R_e(a.u.) and dissociation energies $D_e(cm^{-1})$ with respect to adiabatic products, for $^{1,3}\Pi$ and $^{1,3}\Delta$ states of KH.

State	R_e	D_e
B 1Π	5.34	801
$2\ ^1\Pi$	5.27	1390
$3\ ^1\Pi$	5.57	525
$4\ ^1\Pi$	5.44	740
$5\ ^1\Pi$	5.69	597
$b\ ^3\Pi$	5.77	301
$2\ ^3\Pi$	5.71	333
$3\ ^3\Pi$	5.68	464
$4\ ^3\Pi$	5.71	439
$5\ ^3\Pi$	5.64	540
$1\ ^1\Delta$	5.68	390
$2\ ^1\Delta$	5.65	462
$3\ ^1\Delta$	5.64	514
$1\ ^3\Delta$	5.66	404
$2\ ^3\Delta$	5.67	462
$3\ ^3\Delta$	5.64	512

Let us consider the diabatic results. This is the first *ab initio* evaluation of the dipole moments for the diabatic states of KH. As expected, similarly to LiH,[1] for the dipole of the ionic diabatic state, we get an almost straight line with slope -1 $(-R)$, while the permanent dipole moment of the neutral diabatic states rapidly drops to zero as the internuclear distance increases. This behavior is consistent with a purely ionic diabatic state and confirms the validity of our diabatization approach. The two diabatization methods lead to somewhat different dipole moments mainly at short distances, for the neutral diabatic states. Method 2 which was shown to yield lower residual radial couplings (i.e., states closer to strictly diabatic states), leads also to globally smaller permanent dipoles for the neutral states.

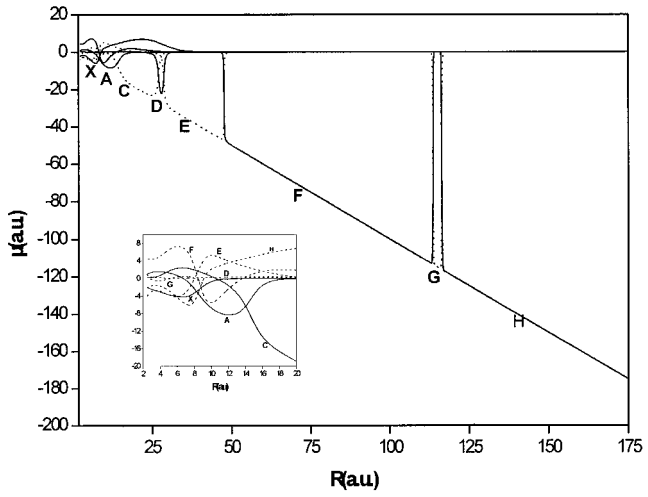

FIG. 11. Permanent dipole moments (μ) for the eight low-lying $^1\Sigma^+$ states of the KH molecule, as a function of the internuclear distance (a.u.); alternating solid and dashed lines correspond to X, A, C, D, E, F, G, and H states; enlarged curves at short distances in the insert.

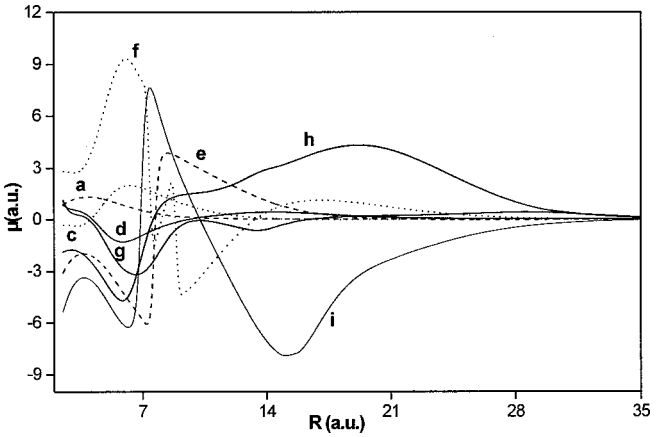

FIG. 12. Permanent dipole moment for the eight low-lying $^3\Sigma$ states, as a function of the internuclear distance (all in a.u.).

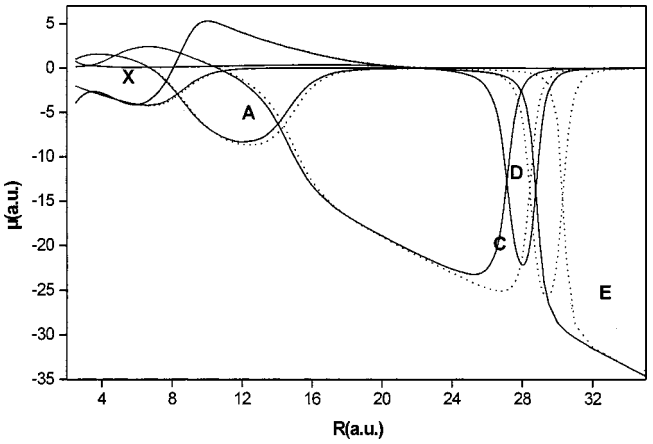

FIG. 14. Permanent dipole moments X, A, C, D, and E, with (dotted line) and without (solid line) the hydrogen electron affinity correction, as a function of the internuclear distance (all in a.u.).

For the adiabatic representation we observe that, one after another, each adiabatic state has its dipole moment that reaches the $-R$ curve and then drops to zero. When combined, these curves reproduce piece-wise the whole $-R$ curve characteristic of the ionic dipole moment and cross forming nodes between consecutive pieces. The curves seem to relay each other to this $-R$ line. This particular behavior can be easily understood from the diabatic potential and dipole moments curves. The permanent dipole gives actually a direct illustration of the ionic character of the adiabatic electronic wavefunction. We thus access directly to a visualization of the R dependence of the charge distribution of the wavefunction. The distance for which two consecutive adiabatic states have the same dipole locates the crossing of the ionic diabatic state with the corresponding neutral one. The sharpness of the slope around the node for the dipole moment is closely related to the weakness of the avoided crossing for energy.

Here again, taking the benefit of the diabatic representation it is possible to improve the results. Without any modification of the dipole moment matrix in the diabatic representation, but using now the previously determined adiabatic–diabatic unitary transformation which involves the corrected ionic curve, we get improved results for the permanent and transition dipole moments. The improved permanent dipoles for the X, A, C, D, and E states are illustrated in Fig. 14 with dotted lines, together with the uncorrected *ab initio* results. The results are consistent with the previous analysis, the crossings being shifted to larger internuclear distances. Interestingly, since the experimental levels spacings of the A state are bracketed by our results with and without the correction of the ionic curve, it can be expected that the exact permanent dipoles are also bracketed by the full and dotted lines reported in Fig. 14, lying closer to the improved results (dotted lines).

Although not affected by the ionic state, the permanent dipoles of the $^3\Sigma^+$ states are not flat curves, as can be seen in Fig. 12, showing the important interplay between the neutral states, consistent with our previous findings.[13,20,36]

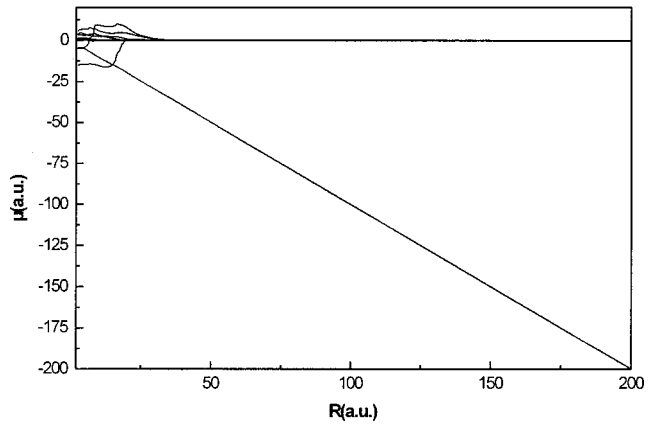

FIG. 13. Permanent diabatic (method 2) dipole moment for the eight low-lying $^1\Sigma$ states of the KH molecule, as a function of the internuclear distance (all in a.u.).

B. Transition dipole moment in adiabatic and diabatic representations

It is interesting to illustrate the behavior of the transition dipole moments in the diabatic and adiabatic representations. All of them cannot be shown here since there are $n(n-1)/2$ curves, with $n=9$ for the $^1\Sigma^+$ states and $n=8$ for the $^3\Sigma^+$ states. Since the adiabatic states present strong variations of their physical electronic characteristics while the diabatic states do not, it is not easy to follow their physical insight with a very restricted number of states. We have selected a few ones, in $^1\Sigma^+$ symmetry, illustrating neutral–ionic crossings and another few illustrating neutral–neutral crossings. Adiabatic transition dipole moments are illustrated in Fig. 15 for the coupled pairs X–A, X–C, A–C, and C–D. Diabatic transition dipole moments are illustrated in Fig. 16 for the coupled pairs ionic–4s, ionic–4p, $4s-4p$, and $5s-3d$.

These adiabatic transition dipoles are imprinted by the ionic curves as can be seen by their changes when the ionic curve is modified (improved results using the ionic curve corrected for the asymptotic H electron affinity error are reported with dots in Fig. 15). Consistently with the A–C potential curves avoided crossing around 15 bohr and also with

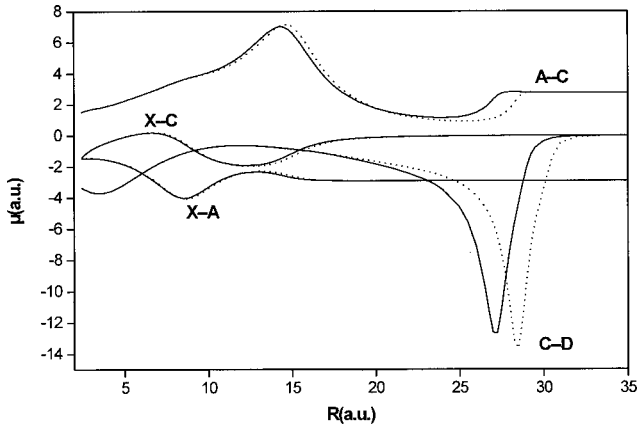

FIG. 15. Transition adiabatic dipole moment X–A, X–C, A–C, and C–D with (dotted line) and without (solid line) a hydrogen electron affinity correction, as a function of the internuclear distance (all in a.u.).

the related crossing of the permanent dipoles of the A and C states, the X–A and X–C transition dipole present an avoided crossing at these distances while the A–C transition dipole shows a peak. This behavior can be understood recalling that, around 15 bohr, the A and C states exchange their ionic character while the X state keeps its 4*s* character. This change in the electronic wavefunction generates a peak in the A–C transition dipole around 15 bohr as it does also for the radial coupling. Similarly, the large peak in the C–D transition dipole curve is related to the C–D potential curves avoided crossing around 27 bohr, being less avoided, the peak is less wide and higher compared to the A–C case. A similar peak is expected for the radial coupling, as was found for LiH.[13] The behavior of these transition dipole moment matrix elements illustrates the well known relation between radial coupling and dipole operators, the relation which allowed in a different context the introduction of the electron translation factors.

Asymptotically, the X, A, C, and D states reach the 4*s*, 4*p*, 5*s*, and 3*d* potassium atomic states, respectively, and the transition dipole moments reach the corresponding atomic transitions. As can be seen in Fig. 16, a similar asymptotic behavior is reached with the diabatic states; however, the transition dipole moments of the diabatic states are dominated by their asymptotic limit over a wide range of internuclear distances and no peak arises, all curves behave much more smoothly compared to the adiabatic case.

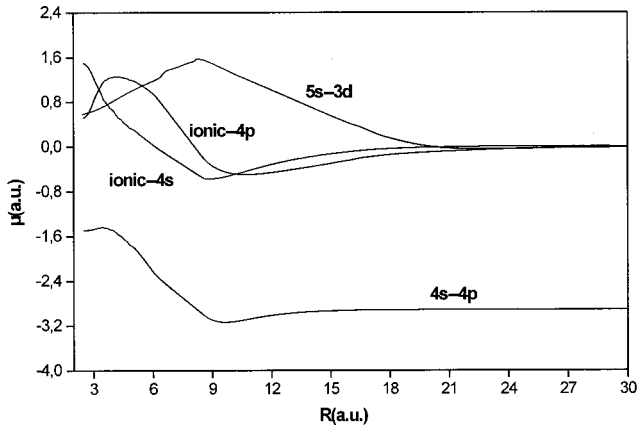

FIG. 16. Transition diabatic dipole moment (method 2): ionic–4*s*, ionic–4*p*, 4*s*–4*p*, and 5*s*–3*d*, as a function of the internuclear distance (all in a.u.).

V. EXPERIMENTAL SUGGESTIONS

The rather unusual behavior of the excited adiabatic $^1\Sigma^+$ states could lead to interesting effects accessible to spectroscopic experimental techniques. There are experimental results on the X and $A\ ^1\Sigma^+$ states only,[10] nothing on the higher ones. However, as for LiH, all of them present a well nearly as deep as the interval between the asymptotic levels. The well minimum moves towards larger interatomic distances as one goes higher in the series and the large distance branch of the well is due to the ionic curve which becomes flatter and flatter as $1/R$. Because of their wide extension, these wells trap a huge number of vibrational levels. In addition to this principal well, which exists for all states whose asymptote is below the ionic (K^+H^-) one, there are also other wells, less deep and at short interatomic nuclear distances. In particular, the E and F states present such a well in the Franck–Condon zone of the ground state and could thus be accessible by photoexcitation. The shape of these double wells suggests interesting spectroscopy and dynamics. Since these highly excited states are embedded in a manifold of continua and bound states, strong vibronic effects can be also expected, as predicted[12,20] and observed[37] for LiH. Work is in progress to determine, with the help of the present diabatic and adiabatic data, conventional and beyond Born–Oppenheimer spectroscopy, including radiative and nonradiative lifetimes, adiabatic corrections and vibronic shifts.

Another interesting point is that the *R* dependence of the dipole moments can be experimentally derived if the expectation value of the dipole is measured for a sufficiently large number of vibrational levels. Thus, when measured for various adiabatic states, such information should lead to an experimental determination of the diabatic neutral–ionic crossing and to the related avoided crossings for the potential curves. Another interesting aspect of the present results is related to the outer repulsive branch of the wells of the excited states, corresponding to the ionic species. It exhibits a considerable dipole moment (a few tenths in a.u.) due to the prominent charge separation in the ionic state. These unusually large values for the dipole moments should lead to interesting physical effects and to signatures, in particular, for the infrared spectrum.

VI. CONCLUSIONS

Accurate adiabatic and diabatic potential curves have been derived for the ground and excited states of the KH molecule. They result form the use of nonempirical pseudopotential allowing for large basis sets, full valence CISD techniques, operatorial core–valence correlation, and efficient diabatization procedure which permit reliable corrections.

In addition to the ground state and first excited states whose accuracy is much better than 1% for almost all bond distances and dissociation energies, we present results for all

curves dissociating below the ionic K^+H^- limit (i.e., 4*s*, 4*p*, 5*s*, 3*d*, 5*p*, 4*d*, 6*s*, and 4*f*). These excited states are probably described with a similar accuracy. Vibrational spacings of the A states are bracketed by our results with and without the H electron affinity correction, which underlines the strong imprint of the A state by the ionic diabatic state.

The intriguing shape of the diabatic neutral curves has been analyzed and interpreted from physical arguments. In our study we emphasize the importance of the accuracy of the ionic state and indeed of the H electron affinity in order to get accurate spectroscopic constants as fundamental as the binding energy of the ground state or the vibrational spacing for the A state.

We have also presented the permanent dipole moments of KH, in both the adiabatic and diabatic representations, for a complete manifold of low-lying $^1\Sigma^+$ states and for a large range of internuclear distances. For the diabatic ionic state, the dipole moment behaves as a straight line. For the adiabatic states, we have curves which relay each other to this line, illustrating their ionic imprint. These results can be easily understood from the physical nature of the diabatic states and they shed light on the interplay between the ionic and neutral species that dominate the alkali hydride potential curves. Consequently, we suggest the possibility of an experimental verification for the location and width of these avoided crossings.

[1] A. Boutalib and F. X. Gadea, J. Chem. Phys. **97**, 1144 (1992).
[2] B. Lepetit, M. LeDourneuf, J. M. Launay, and F. X. Gadea, Chem. Phys. Lett. **135**, 377 (1987).
[3] G. Chanbaud and B. Lévy, J. Phys. B **22**, 3155 (1989).
[4] M. Pelissier, N. Komiha, and J. P. Daudey, J. Comput. Chem. **9**, 298 (1988).
[5] C. L. Peckeris, Phys. Rev. **126**, 1470 (1962).
[6] J. P. Malrieu, D. Maynau, and J. P. Daudey, Phys. Rev. B **30**, 1817 (1984).
[7] V. M. Garcia, R. Caballol, and J. P. Malrieu, J. Chem. Phys. **109**, 504 (1998).
[8] G. H. Jeung, J. P. Daudey, and J. P. Malrieu, J. Phys. B **16**, 699 (1983).
[9] W. C. Stwalley and W. T. Zemke, J. Chem. Ref. Data **22**, 87 (1993).
[10] W. C. Stwalley, W. T. Zemke, and S. C. Yang, J. Chem. Ref. Data **20**, 153 (1991).
[11] H. S. Lee, Y. S. Lee, and G. H. Jeung, Chem. Phys. Lett. **325**, 46 (2000).
[12] F. Gemperle and F. X. Gadea, J. Chem. Phys. **110**, 11197 (1999).
[13] F. X. Gadea and A. Boutalib, J. Phys. B **26**, 61 (1993).
[14] H. Berriche and F. X. Gadea, Chem. Phys. Lett. **247**, 85 (1995).
[15] H. Croft, A. S. Dickinson, and F. X. Gadea, J. Phys. B **32**, 81 (1999).
[16] H. Croft, A. S. Dickinson, and F. X. Gadea, Mon. Notices R. Astron. Soc. **304**, 327 (1999).
[17] A. S. Dickinson and F. X. Gadea, Mon. Notices R. Astron. Soc. **318**, 1227 (2000).
[18] F. X. Gadea, F. Gemperle, H. Berriche, P. Villarreal, and G. Delgado-Barrio, J. Phys. B **30**, L427 (1997).
[19] F. X. Gadea, H. Berriche, O. Roncero, P. Villarreal, and G. Delgado-Bario, J. Chem. Phys. **107**, 10515 (1997).
[20] F. Gemperle and F. X. Gadea, Europhys. Lett. **48**, 513 (1999).
[21] A. Yiannopoulou, G. H. Jeung,, H. S. Lee, and Y. S. Lee, Phys. Rev. A **59**, 1178 (1999).
[22] A. S. Dickinson, R. Poteau, and F. X. Gadea, J. Phys. B **32**, 5451 (1999).
[23] T. Leininger, F. X. Gadea, and A. S. Dickinson, J. Phys. B **33**, 1805 (2000).
[24] R. Cote, M. J. Jamieson, Z. C. Yan, N. Geu, G. H. Jeung, and A. Dalgarno, Phys. Rev. Lett. **84**, 2806 (2000).
[25] W. Müller, J. Flesh, and W. Meyer, J. Chem. Phys. **80**, 3297 (1984).
[26] Ph. Durand and J. C. Barthelat, Theor. Chim. Acta **38**, 283 (1975); J. C. Barthelat and Ph. Durand, Gazz. Chim. Ital. **108**, 225 (1978).
[27] M. Foucrault, Ph. Millie, and J. P. Daudey, J. Chem. Phys. **96**, 1257 (1988).
[28] C. E. Moore, Atomic Energy Levels, NBS (USGPO, Washington, 1971).
[29] F. X. Gadea, thèse d'état, Université Paul Sabatire, Tóulouse, 1987.
[30] F. X. Gadea and M. Pelissier, J. Chem. Phys. **93**, 545 (1990).
[31] T. Romero, A. Aguilar, and F. X. Gadea, J. Chem. Phys. **110**, 6219 (1999).
[32] F. X. Gadea, Phys. Rev. A **43**, 1160 (1991).
[33] R. Hoffmann, J. Chem. Phys. **39**, 1397 (1963).
[34] E. Fermi, Nuovo Cimento **11**, 157 (1934).
[35] A. Omont, J. Phys. (Paris) **38**, 1343 (1977).
[36] A. S. Dickinson and F. X. Gadea, Phys. Rev. A (submitted).
[37] H. Huang, W. T. Luh, G. H. Jeung, and F. X. Gadea, J. Chem. Phys. **113**, 683 (2000).